

# Probing Bulk Band Topology from Time Boundary Effect in Synthetic Dimension

Huisheng Xu,<sup>1</sup> Zhaohui Dong,<sup>2</sup> Luqi Yuan,<sup>2,\*</sup> and Liang Jin<sup>1,†</sup>

<sup>1</sup>*School of Physics, Nankai University, Tianjin 300071, China*

<sup>2</sup>*State Key Laboratory of Advanced Optical Communication Systems and Networks, School of Physics and Astronomy, Shanghai Jiao Tong University, Shanghai, 200240, China*

An incident wave at a temporal interface, created by an abrupt change in system parameters, generates time-refracted and time-reflected waves. We find topological characteristics associated with the temporal interface that separates distinct spatial topologies and report a novel bulk-boundary correspondence for the temporal interface. The vanishing of either time refraction or time reflection records a topological phase transition across the temporal interface, and the difference of bulk band topology predicts nontrivial braiding hidden in the time refraction and time reflection coefficients. These findings, which are insensitive to spatial boundary conditions and robust against disorder, are demonstrated in a synthetic frequency lattice with rich topological phases engendered by long-range couplings. Our work reveals the topological aspect of temporal interface and paves the way for using the time boundary effect to probe topological phase transitions and topological invariants.

*Introduction.*—A temporal interface is the boundary in the time domain where the system parameters undergo an abrupt change. The propagating electromagnetic wave at the temporal interface separating two spatially homogeneous media experiences time refraction and time reflection, governed by a temporal analog of Snell’s law based on the space-time duality of Maxwell’s equations [1–3]. Scattering at the temporal interface resembles that at a spatial interface. Momentum (Energy) is conserved before and after the temporal (spatial) interface due to translational symmetry in space (time) [4, 5]. Thus, a change in the momentum of an incident wave at the spatial interface becomes a change in the energy of the wave at the temporal interface. However, an ideal temporal interface requires a rapid change in the system within a duration much shorter than the wave dynamics, which is extremely challenging to achieve in real materials. Recent experimental advancements underscore the significant potential of fabricating temporal interfaces. Although first observed for classical water wave [6], the temporal interface for optical wave was later realized in an epsilon-near-zero medium [7, 8] and more recently demonstrated for microwave [9, 10] and acoustic wave [11].

Nowadays, the monolayer temporal interface opens up new opportunities for manipulating the electromagnetic waves in the time domain [12, 13]. An immediate application is broadband frequency translation [7, 9]. The interference of time-refracted and time-reflected waves from the multilayer temporal interfaces realizes nonreciprocal [14], reconfigurable [15], and coherent control [16, 17]. Furthermore, periodically and abruptly modulating the refractive index in time constructs photonic time crystals [18–20], which support nontrivial momentum band topology [21]. Temporal topological interface states within the momentum band gap are then identified as the time-domain counterparts of spatial topological interface states [22–24]. This indicates a temporal analog of the bulk-boundary correspondence [25, 26], which is a

fundamental principle of topological phases of matter: a topological invariant characterizes the bulk band topologies of topological phases and predicts interface states at the boundary separating regions with distinct band topologies [27–30]. Although spatial (temporal) topological interface states arising from distinct band topologies in the spatial (temporal) domain have been reported, to the best of our knowledge, the temporal interface of a topological system in the spatial domain remains unexplored. Recently, such a temporal interface in the Su-Schrieffer-Heeger lattice [31] was realized experimentally with ultracold atoms, demonstrating the temporal analog of Snell’s law [32, 33]. Now the question is what topological characteristics are associated with the temporal interface that separates distinct spatial topologies.

Here, we showcase a novel bulk-boundary correspondence for such temporal interfaces. The time refraction or time reflection vanishes at the momentum of the degenerate point, associated with the topological phase transition across the temporal interface. Furthermore, the time refraction and time reflection coefficients braid in the Brillouin zone, and their linking number equals the difference in the winding numbers across the temporal interface. Consequently, the time boundary effect can probe topological phase transition and band topology, fundamentally different from directly measuring the bulk topological invariants [34–42] and the edge states [43–46]. Our findings are demonstrated in a synthetic frequency lattice, where frequency space is analogous to spatial space [47–53]. We highlight the robustness of topological characteristics hidden in the time boundary effect. This work creates new opportunities for the time boundary effect in topological photonics.

*Topological effects for temporal interface.*—The temporal interface of a two-band photonic lattice in the spatial domain splits the incoming light wave into two components [Fig. 1(a)]: a time-refracted wave that propagates in the same direction, and a time-reflected wave that propagates in the opposite direction [54]. The energy

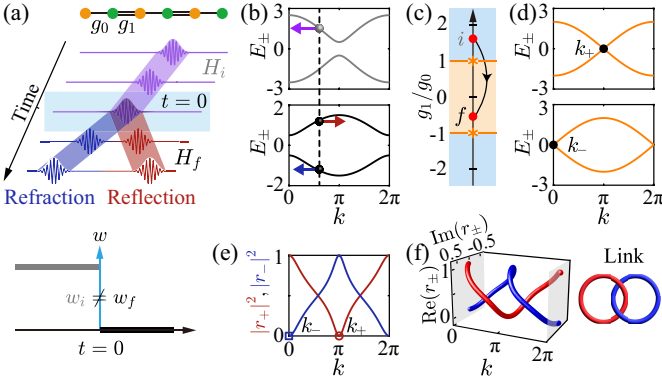


FIG. 1. Probing bulk band topology from the time boundary effect in the Su-Schrieffer-Heeger model. The temporal interface is at  $t = 0$ . The couplings before (after) the temporal interface are  $g_0 = 1$ ,  $g_1 = 1.5$  ( $g_0 = 1$ ,  $g_1 = -0.5$ ). (a) Time refraction and reflection at the temporal interface. (b) Energy bands before (gray) and after (black) the temporal interface. (c) Phase diagram. Topological phase transition occurs at  $g_1 = \pm g_0$  in orange. (d) Energy bands at  $g_1 = g_0$  (upper panel) and  $g_1 = -g_0$  (lower panel). (e) Zeros in  $r_+(k)$  and  $r_-(k)$  at the band gap closing degenerate points  $k_+$  and  $k_-$ . (f) Braiding of  $r_+(k)$  and  $r_-(k)$ .

bands and eigenstates of the Bloch Hamiltonian  $H(k)$  of the two-band photonic lattice are denoted by  $E_{\pm}(k)$  and  $|\psi_{\pm}(k)\rangle$ , where  $k$  is the momentum, and the subscript  $+$  ( $-$ ) represents the upper (lower) band. Furthermore, we use additional subscripts  $i$  and  $f$  in  $H(k)$ ,  $E_{\pm}(k)$ , and  $|\psi_{\pm}(k)\rangle$  to denote the Bloch Hamiltonians, energy bands, and eigenstates before and after the temporal interface, respectively. Without loss of generality, we choose the upper band  $|\psi_{i,+}(k)\rangle$  as the initial excitation arriving at the temporal interface. Then, the time evolution is  $|\Psi(t)\rangle = r_+(k)e^{-iE_{f,+}(k)t}|\psi_{f,+}(k)\rangle + r_-(k)e^{-iE_{f,-}(k)t}|\psi_{f,-}(k)\rangle$ . The projections  $r_{\pm}(k)$  yield the time refraction and reflection coefficients

$$r_+(k) = \langle \psi_{f,+}(k) | \psi_{i,+}(k) \rangle, r_-(k) = \langle \psi_{f,-}(k) | \psi_{i,+}(k) \rangle. \quad (1)$$

The total probability is unity  $|r_+(k)|^2 + |r_-(k)|^2 = 1$  [32, 54]. The velocities of time refraction and reflection are predicted by  $dE_{f,\pm}(k)/dk$  [Fig. 1(b)].

When the Bloch Hamiltonians  $H_i(k)$  and  $H_f(k)$  share identical eigenstates, the orthogonality between their eigenstates results in the vanishing of time refraction or time reflection. This occurs at the momentum of the band gap closing degenerate point associated with the topological phase transition across the temporal interface (Supplemental Material A [55]). Notably, the topological phases chosen before and after the temporal interface are represented by two red dots in the phase diagram [Fig. 1(c)]. The straight line connecting the two red dots intersects the topological phase boundaries at two orange asterisks. At the orange asterisk inside (outside) the two red dots, the band gap closes at the momentum  $k_+$  ( $k_-$ )

[Fig. 1(d)], where  $r_+(k)$  [ $r_-(k)$ ] reaches zero [Fig. 1(e)]. Thus, the zeros in the time refraction and time reflection record the topological phase transitions. Furthermore, when the topological phases before and after the temporal interface are adjacent in the phase diagram, the minimal number of zeros in  $r_+(k)$  and  $r_-(k)$  determines the minimal number of degenerate points encountered during their topological phase transition. These degenerate points are associated with changes in the band topology. This allows the detection of topological invariant in the phase diagram tomograph by counting zeros in  $r_+(k)$  and  $r_-(k)$ .

The synthetic frequency lattice with chiral symmetry enables the visualization of topological effects emerging from the temporal interface. The associated Bloch Hamiltonian has an off-diagonal form

$$H(k) = \begin{pmatrix} 0 & \mathcal{G}^\dagger(k) \\ \mathcal{G}(k) & 0 \end{pmatrix}. \quad (2)$$

The eigenenergies are  $E_{\pm}(k) = \pm|\mathcal{G}(k)|$ , and the eigenstates are  $|\psi_{\pm}(k)\rangle = (1, \pm e^{i\varphi(k)})^T/\sqrt{2}$ , where  $\varphi(k) = \arg[\mathcal{G}(k)]$ . The topological phase before (after) the temporal interface is characterized by the winding number  $w_{i(f)} = (2\pi)^{-1} \int_0^{2\pi} \partial_k \varphi_{i(f)}(k) dk$ , which is the number of times the complex  $\mathcal{G}_{i(f)}(k)$  winds around the origin [25]. The time refraction and reflection coefficients are  $r_{\pm}(k) = \{1 \pm e^{i[\varphi_i(k) - \varphi_f(k)]}\}/2$ . The complex  $r_+(k)$  and  $r_-(k)$  braid in the  $\text{Re}[r_{\pm}(k)]$ - $\text{Im}[r_{\pm}(k)]$ - $k$  space [Fig. 1(f)]. After mapping the entire period  $k \in [0, 2\pi]$  of  $r_{\pm}(k)$  onto a torus by taking  $k$  as the toroidal direction,  $r_+(k)$  and  $r_-(k)$  become two closed curves that form a link. The linking number equals the difference in the winding numbers across the temporal interface (Supplemental Material B [55])

$$\mathcal{L} = w_i - w_f. \quad (3)$$

Thus, the time boundary effect can extract the difference in winding numbers across the temporal interface. Probing bulk band topology through time boundary effect differs from directly measuring the Zak phase [56].

The topological characteristics hidden in the time boundary effect reveal the bulk-boundary correspondence for the temporal interface that separates distinct spatial topologies, including (i) the vanishing of time refraction or time reflection at the momentum of the band gap closing degenerate point, and (ii) the braiding of time refraction and reflection arising from distinct spatial topologies. These features uncover the topological phase transition and the winding numbers across the temporal interface.

*Rich topological phases.*—We propose a concrete synthetic frequency lattice that supports rich topological phases with high winding numbers to demonstrate the bulk-boundary correspondence for the temporal interface. The multiplicity of band topologies is enriched

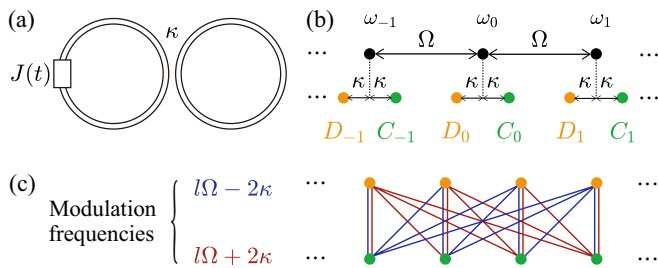


FIG. 2. (a) Coupled ring resonators. (b) The frequencies of symmetric (green dots) and anti-symmetric (orange dots) supermodes. (c) Schematic of the effective couplings created by the modulation frequencies in the sinusoidal modulation  $J(t)$ . The associated  $H(k)$  has the form of Eq. (2).

by incorporating long-range couplings [57–63], which are typically weak or negligible due to the exponential decay of evanescent fields [64, 65]. The synthetic frequency dimension offers a feasible platform for studying topological physics with long-range couplings [66–69].

We consider two identical ring resonators coupled with strength  $\kappa$  [Fig. 2(a)]. Each ring resonator supports a set of equally-spaced resonant frequency modes  $\omega_n = \omega_0 + n\Omega$  ( $n \in \mathbb{Z}$ ) that differ by the free spectral range  $\Omega$  [47], where  $\omega_0$  is the central frequency. The coupling  $\kappa$  results in symmetric supermodes  $\omega_n + \kappa$  and antisymmetric supermodes  $\omega_n - \kappa$  [Fig. 2(b)] [41, 42, 51]. An electro-optic phase modulator is placed inside one of the two rings with an external modulation  $J(t)$ . The sinusoidal modulation of the refractive index in the ring resonator can establish connectivity between the supermodes [41]. The spacing of the connectivity depends on the modulation frequency, while the coupling strength is determined by the modulation amplitude, enabling the realization of long-range couplings by choosing the modulation frequency as a multiple of free spectral range [67, 70, 71]. The synthetic frequency lattice is a ladder as illustrated in Fig. 2(c). The modulation frequencies  $l\Omega - 2\kappa$  (blue) and  $l\Omega + 2\kappa$  (red) lead to the inter-ladder-leg couplings, which appear as off-diagonal terms in  $H(k)$  (Supplemental Material C [55]). The indices  $l = 0$ ,  $|l| = 1$ , and  $|l| > 1$  are integers, and the associated modulations generate vertical coupling, nearest-neighbor coupling, and long-range coupling, respectively [42].

We focus on a polychromatic modulation  $J(t) = \sum_l 4g_l \cos[(l\Omega - 2\kappa)t + \phi_l]$ . The corresponding Bloch Hamiltonian  $H(k)$  is Eq. (2) with  $\mathcal{G}(k) = \sum_l g_l e^{i\phi_l} e^{ikl}$ , preserving chiral symmetry. In the ten-fold way classification of topological phases [72],  $H(k)$  belongs to class BDI for  $\phi_l = m\pi$  ( $m \in \mathbb{Z}$ ), preserving additional time-reversal symmetry and particle-hole symmetry; and  $H(k)$  belongs to class AIII for  $\phi_l \neq m\pi$  ( $m \in \mathbb{Z}$ ), where the phase factor  $\phi_l$  creates a gauge field and affects the band topology. Both classes feature a  $\mathbb{Z}$  topological invariant [73]. The winding number  $w$  characterizes the band

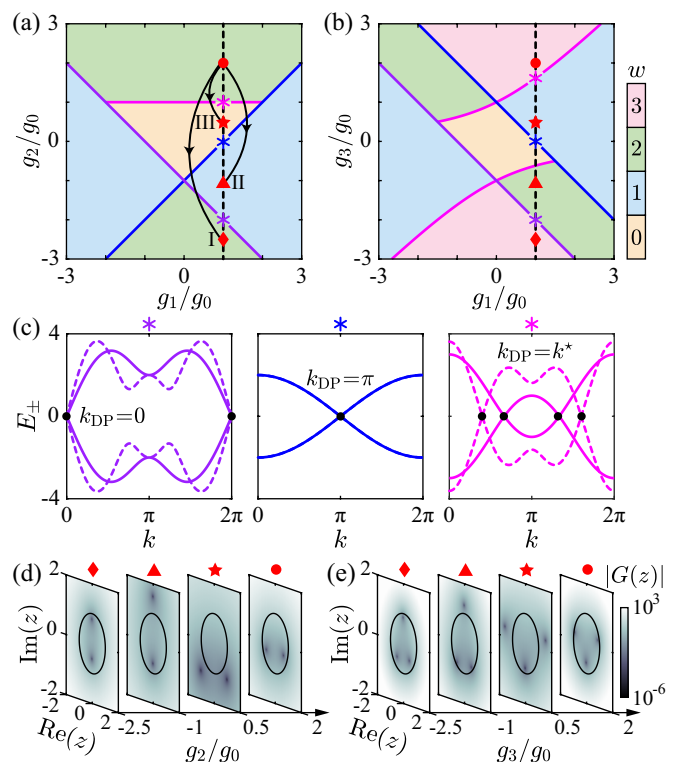


FIG. 3. Phase diagrams for the synthetic frequency lattice with long-range coupling: (a)  $g_2$  and (b)  $g_3$ . (c) Energy bands at the asterisks on different phase boundaries. The solid and dashed lines are for (a) and (b), respectively.  $k^* = \arccos[-g_1/(2g_2)]$  for (a) and  $k^* = \arccos[g_0/(2g_3)]$  for (b). (d) and (e)  $|G(z)|$  for the red diamond, triangle, star, and dot in (a) and (b). The black ellipse represents the unit circle.

topology. According to Cauchy’s argument principle,  $w$  equals the number of zeros minus the order of pole from  $G(z) = \sum_l g_l e^{i\phi_l} z^l$  in the complex plane  $z$ , within the unit circle (i.e.,  $z = e^{ik}$ ). We discuss the scenario  $\phi_l = 0$ , and other scenarios can be treated similarly.

A bichromatic modulation  $J(t)$  with  $g_0, g_1 \neq 0$  constructs the Su-Schrieffer-Heeger model [41], which supports a topologically trivial phase ( $w = 0$ ) and a topologically nontrivial phase ( $w = 1$ ). The long-range coupling  $g_l$  with index  $|l| > 1$  creates topologically nontrivial phases with high winding numbers [42]. The phase diagrams for the trichromatic modulation  $J(t)$  with  $g_0, g_1, g_2 \neq 0$  and  $g_0, g_1, g_3 \neq 0$  are displayed in Figs. 3(a) and 3(b) (Supplemental Material D [55]). At topological phase transitions [colored asterisks in Figs. 3(a) and 3(b)], the band gap closes at the degenerate points of the energy bands [black dots in Fig. 3(c)], which are associated with a change in the band topology. The different topologies in Figs. 3(a) and 3(b), obtained from  $|G(z)|$ , are shown in Figs. 3(d) and 3(e), where the pole is absent and the number of zeros within the unit circle indicates the winding number of each phase.

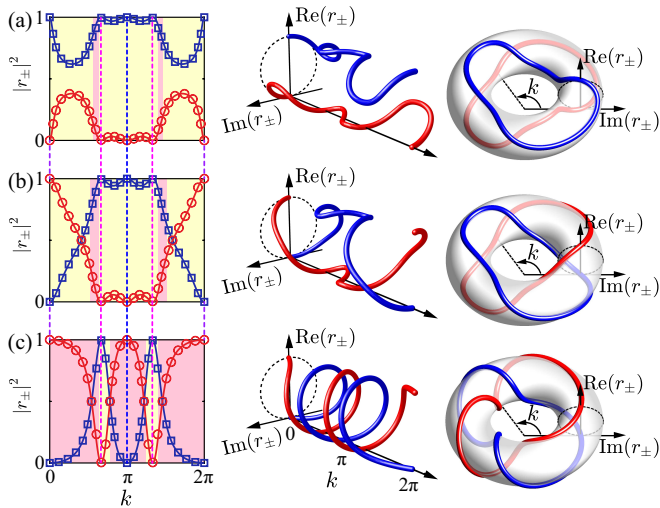


FIG. 4. The plots of  $r_+(k)$  (red curve) and  $r_-(k)$  (blue curve). As illustrated in Fig. 3(a), the topological phases across the time boundary lie along the dashed black line  $g_1 = g_0$ . The topological phase before the time boundary at  $g_2 = 2g_0$  (red dot) has  $w_i = 2$ , while the topological phases after the time boundary, at (a)  $g_2 = -5g_0/2$  (red diamond), (b)  $g_2 = -g_0$  (red triangle), and (c)  $g_2 = g_0/2$  (red star) for case I, II, and III, have  $w_f = 2$ ,  $w_f = 1$ , and  $w_f = 0$ , respectively. Here,  $r_+(k)$  represents time refraction (reflection), and  $r_-(k)$  represents time reflection (refraction) within the pink (yellow) region (Supplemental Material E [55]). The markers correspond to numerical simulations [74]. The toroidal direction of the torus is the one-dimensional excitation momentum  $k$ . The cross section of the torus is  $r_{\pm}(k)$ .

*Topological time boundary.*—We demonstrate the detection of bulk band topology from the time boundary effect. Topological phases before and after the time boundary, for the examples shown in Fig. 4, are selected on the dashed black line in the phase diagram of Fig. 3(a). This dashed black line intersects the topological phase boundaries at the colored asterisks. The band gap of  $H(k)$  at the purple, blue, and magenta asterisks closes at the degenerate points with the momenta  $k_{\text{DP}} = 0$ ,  $k_{\text{DP}} = \pi$ , and  $k_{\text{DP}} = 2\pi/3, 4\pi/3$ , respectively, as shown in Fig. 3(c). In Fig. 4 (left panel), a remarkable feature is the vanishing of time refraction or time reflection at these momenta. The dashed lines indicate these zeros, using the colors of the corresponding topological phase boundaries. Notably, these zeros, considered collectively, are identical in all three cases, but their distributions in  $r_+(k)$  and  $r_-(k)$  are different.

Case I experiences all the purple, blue, and magenta topological phase transitions [Fig. 3(a)]. As a result, all the zeros at  $k_{\text{DP}} = 0$ ,  $k_{\text{DP}} = \pi$ , and  $k_{\text{DP}} = 2\pi/3, 4\pi/3$  appear in  $r_+(k)$  [Fig. 4(a)]. Similarly, case II experiences the blue and magenta topological phase transitions [Fig. 3(a)]. Consequently, the zeros at  $k_{\text{DP}} = \pi$  and  $k_{\text{DP}} = 2\pi/3, 4\pi/3$  appear in  $r_+(k)$ , while the zero

at  $k_{\text{DP}} = 0$  appears in  $r_-(k)$  [Fig. 4(b)]. Finally, case III experiences the magenta topological phase transition [Fig. 3(a)]. Thus, the zeros at  $k_{\text{DP}} = 2\pi/3, 4\pi/3$  appear in  $r_+(k)$ , and the zeros at  $k_{\text{DP}} = 0$  and  $k_{\text{DP}} = \pi$  appear in  $r_-(k)$  [Fig. 4(c)]. Furthermore, the interchange of zeros between  $r_+(k)$  and  $r_-(k)$  signifies a topological phase transition, and the associated momentum pinpoints the location of degenerate point. In comparison with the zeros in Figs. 4(a) and 4(b), the zero at  $k_{\text{DP}} = 0$  in  $r_+(k)$  switches to  $r_-(k)$ . This indicates a topological phase transition, with the band gap closing at  $k_{\text{DP}} = 0$ , and  $w$  changes by 1. In comparison with the zeros in Figs. 4(b) and 4(c), the zero at  $k_{\text{DP}} = \pi$  in  $r_+(k)$  switches to  $r_-(k)$ . This indicates another topological phase transition, with the band gap closing at  $k_{\text{DP}} = \pi$ , and  $w$  changes by 1.

In Fig. 4, the braidings (middle panel) of time refraction and reflection form links (right panel) when mapped onto a torus. Figure 4(a) shows case I, where  $r_+(k)$  and  $r_-(k)$  do not braid, forming an unlink with  $\mathcal{L} = 0$ . Figure 4(b) shows case II, where  $r_+(k)$  and  $r_-(k)$  braid once, forming a Hopf link with  $\mathcal{L} = 1$ . Figure 4(c) shows case III, where  $r_+(k)$  and  $r_-(k)$  braid twice, forming a Solomon link with  $\mathcal{L} = 2$ . These links are topologically inequivalent and cannot be continuously deformed from one to another without untying. The linking number  $\mathcal{L}$  of  $r_+(k)$  and  $r_-(k)$  accurately reflects the variation in the winding number across the time boundary  $w_i - w_f$  [75], as verified from  $w_i = 2$  and  $w_f = 2, 1, 0$  for cases I, II, III. The formation of links, ensured by different winding numbers across the time boundary, gives rise to  $|r_+(k_{\text{DQPT}})|^2 = |r_-(k_{\text{DQPT}})|^2 = 1/2$  for a dynamical quantum phase transition [76]. Thus, the existence of  $k_{\text{DQPT}}$  is topologically protected, and the least number of  $k_{\text{DQPT}}$  in the entire period  $k \in [0, 2\pi]$  is predicted by the link crossing number  $2\mathcal{L}$ , i.e., the minimal number of crossings that occur in any projection of a link. We highlight that the zeros and braidings associated with the time refraction and time reflection are robust to disorder (Supplemental Material F [55]). Thus, the time boundary effect is a versatile tool for phase diagram tomography.

*Conclusion and Discussion.*—The temporal degree of freedom heralds a new era in the control and manipulation of light [77]. The time boundary effect encodes information about bulk band topologies both before and after the temporal interface. We uncover a novel bulk-boundary correspondence for the temporal interface that separates distinct spatial topologies and demonstrate the use of the time boundary effect to probe bulk band topology. The vanishing of either time refraction or time reflection signifies a topological phase transition across the temporal interface, and the braiding of time refraction and time reflection identifies different winding numbers across the temporal interface. Probing topology using the time boundary effect is insensitive to the boundary conditions of the synthetic frequency lattice, as the

dynamics are confined within a finite-size region. Furthermore, the vanishing of time refraction or time reflection also occurs at the topological phase transition across the temporal interface in high-dimensional topological phases [55]. Consequently, the time boundary effect in two-dimensional Chern insulators can probe the topological phase transitions and the Chern numbers [78–83]. Our findings pave the way for future investigations into nonequilibrium [84, 85], non-Abelian [86–88], nonlinear [89–92], and non-Hermitian [93, 94] topologies in spatiotemporal metamaterials [95–97].

This work was supported by National Natural Science Foundation of China (Grants No. 12222504, No. 12122407, No. 124B2079, and No. 12475021), and National Key Research and Development Program of China (2023YFA1407200).

---

\* yuanluqi@sjtu.edu.cn

† jinliang@nankai.edu.cn

- [1] S. Akhmanov, A. Sukhorukov, and A. Chirkin, Nonstationary phenomena and space-time analogy in nonlinear optics, *Sov. Phys. JETP* **28**, 748 (1969).
- [2] B. Kolner, Space-time duality and the theory of temporal imaging, *IEEE J. Quantum Electron.* **30**, 1951 (1994).
- [3] J. Mendonça and P. Shukla, Time refraction and time reflection: Two basic concepts, *Phys. Scr.* **65**, 160 (2002).
- [4] Y. Xiao, D. N. Maywar, and G. P. Agrawal, Reflection and transmission of electromagnetic waves at a temporal boundary, *Opt. Lett.* **39**, 574 (2014).
- [5] B. W. Plansinis, W. R. Donaldson, and G. P. Agrawal, What is the temporal analog of reflection and refraction of optical beams? *Phys. Rev. Lett.* **115**, 183901 (2015).
- [6] V. Bacot, M. Labousse, A. Eddi, M. Fink, and E. Fort, Time reversal and holography with spacetime transformations, *Nat. Phys.* **12**, 972 (2016).
- [7] Y. Zhou, M. Z. Alam, M. Karimi, J. Upham, O. Reshef, C. Liu, A. E. Willner, and R. W. Boyd, Broadband frequency translation through time refraction in an epsilon-near-zero material, *Nat. Commun.* **11**, 2180 (2020).
- [8] J. Bohn, T. S. Luk, S. Horsley, and E. Hendry, Spatiotemporal refraction of light in an epsilon-near-zero indium tin oxide layer: frequency shifting effects arising from interfaces, *Optica* **8**, 1532 (2021).
- [9] H. Moussa, G. Xu, S. Yin, E. Galiffi, Y. Ra’di, and A. Alù, Observation of temporal reflection and broadband frequency translation at photonic time interfaces, *Nat. Phys.* **19**, 863 (2023).
- [10] T. R. Jones, A. V. Kildishev, M. Segev, and D. Peroulis, Time-reflection of microwaves by a fast optically-controlled time-boundary, *Nat. Commun.* **15**, 6786 (2024).
- [11] B. L. Kim, C. Chong, and C. Daraio, Temporal Refraction in an Acoustic Phononic Lattice, *Phys. Rev. Lett.* **133**, 077201 (2024).
- [12] M. S. Mirmoosa, M. H. Mostafa, A. Norrman, and S. A. Tretyakov, Time interfaces in bianisotropic media, *Phys. Rev. Research* **6**, 013334 (2024).
- [13] L. Bar-Hillel, A. Dikopoltsev, A. Kam, Y. Sharabi, O. Segal, E. Lustig, and M. Segev, Time Refraction and Time Reflection above Critical Angle for Total Internal Reflection, *Phys. Rev. Lett.* **132**, 263802 (2024).
- [14] H. Li, S. Yin, and A. Alù, Nonreciprocity and Faraday Rotation at Time Interfaces, *Phys. Rev. Lett.* **128**, 173901 (2022).
- [15] H. Ye, C. Qin, S. Wang, L. Zhao, W. Liu, B. Wang, S. Longhi, and P. Lu, Reconfigurable refraction manipulation at synthetic temporal interfaces with scalar and vector gauge potentials, *Proc. Natl. Acad. Sci. U.S.A.* **120**, e2300860120 (2023).
- [16] E. Galiffi, G. Xu, S. Yin, H. Moussa, Y. Ra’di, and A. Alù, Broadband coherent wave control through photonic collisions at time interfaces, *Nat. Phys.* **19**, 1703 (2023).
- [17] Z. Dong, X. Wu, Y. Yang, P. Yu, X. Chen, and L. Yuan, Temporal multilayer structures in discrete physical systems towards arbitrary-dimensional non-Abelian Aharonov-Bohm interferences, *Nat. Commun.* **15**, 7392 (2024).
- [18] Z. Hayran, J. B. Khurgin, and F. Monticone,  $\hbar\omega$  versus  $\hbar k$ : Dispersion and Energy Constraints on Time-Varying Photonic Materials and Time Crystals, *Opt. Mater. Exp.* **12**, 3904 (2022).
- [19] A. Boltasseva, V. M. Shalaev, and M. Segev, Photonic time crystals: from fundamental insights to novel applications: opinion, *Opt. Mater. Exp.* **14**, 592 (2024).
- [20] M. M. Asgari, P. Garg, X. Wang, M. S. Mirmoosa, C. Rockstuhl, V. Asadchy, Theory and applications of photonic time crystals: a tutorial, *Adv. Opt. Photon.* **16**, 958 (2024).
- [21] E. Lustig, Y. Sharabi, and M. Segev, Topological aspects of photonic time crystals, *Optica* **5**, 1390 (2018).
- [22] K. Giergiel, A. Dauphin, M. Lewenstein, J. Zakrzewski, and K. Sacha, Topological time crystals, *New J. Phys.* **21**, 052003 (2019).
- [23] M.-W. Li, J.-W. Liu, X. Wang, W.-J. Chen, G. Ma, J.-W. Dong, Topological temporal boundary states in a non-Hermitian spatial crystal, [arXiv:2306.09627](https://arxiv.org/abs/2306.09627).
- [24] Y. Ren, K. Ye, Q. Chen, F. Chen, L. Zhang, Y. Pan, W. Li, X. Li, L. Zhang, H. Chen, and Y. Yang, Observation of momentum-gap topology of light at temporal interfaces in a time-synthetic lattice, *Nat. Commun.* **16**, 707 (2025).
- [25] X. G. Wen and A. Zee, Winding numer, family index theorem, and electron hopping in a magnetic field, *Nucl. Phys. B* **316**, 641 (1989).
- [26] Y. Hatsugai, Chern number and edge states in the integer quantum Hall effect, *Phys. Rev. Lett.* **71**, 3697 (1993).
- [27] M. Z. Hasan and C. L. Kane, Colloquium: Topological insulators, *Rev. Mod. Phys.* **82**, 3045 (2010).
- [28] A. Bansil, H. Lin, and T. Das, Colloquium: Topological band theory, *Rev. Mod. Phys.* **88**, 021004 (2016).
- [29] T. Ozawa, H. M. Price, A. Amo, N. Goldman, M. Hafezi, L. Lu, M. C. Rechtsman, D. Schuster, J. Simon, O. Zilberberg, and I. Carusotto, Topological photonics, *Rev. Mod. Phys.* **91**, 015006 (2019).
- [30] H. Price, Y. Chong, A. Khanikaev, H. Schomerus, L. J. Maczewsky, M. Kremer, M. Heinrich, A. Szameit, O. Zilberberg, Y. Yang, B. Zhang, A. Alù, R. Thomale, I. Carusotto, P. St-Jean, A. Amo, A. Dutt, L. Yuan,

- S. Fan, X. Yin, C. Peng, T. Ozawa, and A. Blanco-Redondo, Roadmap on topological photonics, *J. Phys. Photonics* **4**, 032501 (2022).
- [31] W. P. Su, J. R. Schrieffer, and A. J. Heeger, Solitons in Polyacetylene, *Phys. Rev. Lett.* **42**, 1698 (1979).
- [32] Z. Dong, H. Li, T. Wan, Q. Liang, Z. Yang, and B. Yan, Quantum time reflection and refraction of ultracold atoms, *Nat. Photon.* **18**, 68 (2024).
- [33] P. Hannaford and K. Sacha, Reflection and refraction at a time boundary, *Nat. Photon.* **18**, 7 (2024).
- [34] M. Atala, M. Aidelsburger, J. T. Barreiro, D. Abanin, T. Kitagawa, E. Demler, and I. Bloch, Direct measurement of the Zak phase in topological Bloch bands, *Nat. Phys.* **9**, 795 (2013).
- [35] W. Hu, J. C. Pillay, K. Wu, M. Pasek, P. P. Shum, and Y. D. Chong, Measurement of a Topological Edge Invariant in a Microwave Network, *Phys. Rev. X* **5**, 011012 (2015).
- [36] F. Cardano, A. D'Errico, A. Dauphin, M. Maffei, B. Piccirillo, C. de Lisio, G. De Filippis, V. Cataudella, E. Santamato, L. Marrucci, M. Lewenstein, and P. Massignan, Detection of Zak phases and topological invariants in a chiral quantum walk of twisted photons, *Nat. Commun.* **8**, 15516 (2017).
- [37] X.-Y. Xu, Q.-Q. Wang, W.-W. Pan, K. Sun, J.-S. Xu, G. Chen, J.-S. Tang, M. Gong, Y.-J. Han, C.-F. Li, and G.-C. Guo, Measuring the Winding Number in a Large-Scale Chiral Quantum Walk, *Phys. Rev. Lett.* **120**, 260501 (2018).
- [38] Y. Wang, Y.-H. Lu, F. Mei, J. Gao, Z.-M. Li, H. Tang, S.-L. Zhu, S. Jia, and X.-M. Jin, Direct Observation of Topology from Single-Photon Dynamics, *Phys. Rev. Lett.* **122**, 193903 (2019).
- [39] F. N. Ünal, B. Seradjeh, and A. Eckardt, How to Directly Measure Floquet Topological Invariants in Optical Lattices, *Phys. Rev. Lett.* **122**, 253601 (2019).
- [40] Z.-Q. Jiao, S. Longhi, X.-W. Wang, J. Gao, W.-H. Zhou, Y. Wang, Y.-X. Fu, L. Wang, R.-J. Ren, L.-F. Qiao, and X.-M. Jin, Experimentally Detecting Quantized Zak Phases without Chiral Symmetry in Photonic Lattices, *Phys. Rev. Lett.* **127**, 147401 (2021).
- [41] G. Li, L. Wang, R. Ye, Y. Zheng, D.-W. Wang, X.-J. Liu, A. Dutt, L. Yuan, and X. Chen, Direct extraction of topological Zak phase with the synthetic dimension, *Light Sci. Appl.* **12**, 81 (2023).
- [42] F. Pellerin, R. Houvenaghe, W. A. Coish, I. Carusotto, and P. St-Jean, Wave-Function Tomography of Topological Dimer Chains with Long-Range Couplings, *Phys. Rev. Lett.* **132**, 183802 (2024).
- [43] M. Hafezi, S. Mittal, J. Fan, A. Migdall, and J. M. Taylor, Imaging topological edge states in silicon photonics, *Nat. Photon.* **7**, 1001 (2013).
- [44] S. Mittal, S. Ganeshan, J. Fan, A. Vaezi, and M. Hafezi, Measurement of topological invariants in a 2D photonic system, *Nat. Photon.* **10**, 180 (2016).
- [45] L.-C. Wang, Y. Chen, M. Gong, F. Yu, Q.-D. Chen, Z.-N. Tian, X.-F. Ren, and H.-B. Sun, Edge State, Localization Length, and Critical Exponent from Survival Probability in Topological Waveguides, *Phys. Rev. Lett.* **129**, 173601 (2022).
- [46] H. S. Xu, K. L. Zhang, L. Jin, and Z. Song, Signature of edge states in resonant wave scattering, *Phys. Rev. A* **105**, 033501 (2022).
- [47] L. Yuan, Y. Shi, and S. Fan, Photonic gauge potential in a system with a synthetic frequency dimension, *Opt. Lett.* **41**, 741 (2016).
- [48] T. Ozawa, H. M. Price, N. Goldman, O. Zilberberg, and I. Carusotto, Synthetic dimensions in integrated photonics: From optical isolation to four-dimensional quantum Hall physics, *Phys. Rev. A* **93**, 043827 (2016).
- [49] Z. Yang, E. Lustig, G. Harari, Y. Plotnik, Y. Lumer, M. A. Bandres, and M. Segev, Mode-Locked Topological Insulator Laser Utilizing Synthetic Dimensions, *Phys. Rev. X* **10**, 011059 (2020).
- [50] A. Dutt, Q. Lin, L. Yuan, M. Minkov, M. Xiao, and S. Fan, A single photonic cavity with two independent physical synthetic dimensions, *Science* **367**, 59 (2020).
- [51] A. Dutt, M. Minkov, I. A. D. Williamson, and S. Fan, Higher-order topological insulators in synthetic dimensions, *Light Sci. Appl.* **9**, 131 (2020).
- [52] J. Suh, G. Kim, H. Park, S. Fan, N. Park, and S. Yu, Photonic Topological Spin Pump in Synthetic Frequency Dimensions, *Phys. Rev. Lett.* **132**, 033803 (2024).
- [53] G. Villa, I. Carusotto, and T. Ozawa, Mean-chiral displacement in coherently driven photonic lattices and its application to synthetic frequency dimensions, *Commun. Phys.* **7**, 246 (2024).
- [54] O. Y. Long, K. Wang, A. Dutt, and S. Fan, Time reflection and refraction in synthetic frequency dimension, *Phys. Rev. Research* **5**, L012046 (2023).
- [55] Supplemental Material provides a proof of the connection between the zeros in the time refraction (reflection) and the degenerate points from the topological phase transition across the temporal interface, a proof of the equivalence between the linking number of time refraction and reflection mapped onto a torus and the winding number difference across the temporal interface, as well as more details on the synthetic frequency lattice, the phase diagram, the energy bands, and the robustness of topological features in the time boundary effect.
- [56] J. Zak, Berry's phase for energy bands in solids, *Phys. Rev. Lett.* **62**, 2747 (1989).
- [57] D. Leykam, S. Mittal, M. Hafezi, and Y. D. Chong, Reconfigurable topological phases in next-nearest-neighbor coupled resonator lattices, *Phys. Rev. Lett.* **121**, 023901 (2018).
- [58] E. Lustig, S. Weimann, Y. Plotnik, Y. Lumer, M. A. Bandres, A. Szameit, and M. Segev, Photonic topological insulator in synthetic dimensions, *Nature* **567**, 356 (2019).
- [59] W. A. Benalcazar and A. Cerjan, Chiral-Symmetric Higher-Order Topological Phases of Matter, *Phys. Rev. Lett.* **128**, 127601 (2022).
- [60] K. Chen and A. B. Khanikaev, Non-Hermitian  $C_{NH} = 2$  Chern insulator protected by generalized rotational symmetry, *Phys. Rev. B* **105**, L081112 (2022).
- [61] Z. Wang, X. Wang, Z. Hu, D. Bongiovanni, D. Jukić, L. Tang, D. Song, R. Morandotti, Z. Chen, and H. Buljan, Sub-symmetry-protected topological states, *Nat. Phys.* **19**, 992 (2023).
- [62] H. Liu, X. Huang, M. Yan, J. Lu, W. Deng, and Z. Liu, Acoustic Topological Metamaterials of Large Winding Number, *Phys. Rev. Appl.* **19**, 054028 (2023).
- [63] M. Li, D. Zhirihin, M. Gorlach, X. Ni, D. Filonov, A. Slobozhanyuk, A. Alù, and A. B. Khanikaev, Higher-order topological states in photonic kagome crystals

- with long-range interactions, *Nat. Photon.* **14**, 89 (2020).
- [64] G. J. Tang, X. T. He, F. L. Shi, J. W. Liu, X. D. Chen, and J. W. Dong, Topological photonic crystals: Physics, designs, and applications, *Laser Photon. Rev.* **16**, 2100300 (2022).
- [65] M. Kim, Z. Jacob, and J. Rho, Recent advances in 2D, 3D and higher-order topological photonics, *Light Sci. Appl.* **9**, 130 (2020).
- [66] T. Ozawa and H. M. Price, Topological quantum matter in synthetic dimensions, *Nat. Rev. Phys.* **1**, 349 (2019).
- [67] A. Senanian, L. G. Wright, P. F. Wade, H. K. Doyle, and P. L. McMahon, Programmable large-scale simulation of bosonic transport in optical synthetic frequency lattices, *Nat. Phys.* **19**, 1333 (2023).
- [68] K. Wang, A. Dutt, C. C. Wojcik, and S. Fan, Topological complex-energy braiding of non-Hermitian bands, *Nature* **598**, 59 (2021).
- [69] R. Ye, Y. He, G. Li, L. Wang, X. Wu, X. Qiao, Y. Zheng, L. Jin, D.-W. Wang, L. Yuan, and X. Chen, Observing non-Hermiticity induced chirality breaking in a synthetic Hall ladder, *Light Sci. Appl.* **14**, 39 (2025).
- [70] L. Yuan, M. Xiao, Q. Lin, and S. Fan, Synthetic space with arbitrary dimensions in a few rings undergoing dynamic modulation, *Phys. Rev. B* **97**, 104105 (2018).
- [71] D. Cheng, E. Lustig, K. Wang, and S. Fan, Multi-dimensional band structure spectroscopy in the synthetic frequency dimension, *Light Sci. Appl.* **12**, 158 (2023).
- [72] A. Altland and M. R. Zirnbauer, Nonstandard symmetry classes in mesoscopic normal-superconducting hybrid structures, *Phys. Rev. B* **55**, 1142 (1997).
- [73] C.-K. Chiu, J. C. Y. Teo, A. P. Schnyder, and S. Ryu, Classification of topological quantum matter with symmetries, *Rev. Mod. Phys.* **88**, 035005 (2016).
- [74] The initial state is a Gaussian wave packet that excites the eigenstate of the upper band. At the moment  $t = 0$ , the amplitudes of antisymmetric ( $\psi_{D_m}$ ) and symmetric ( $\psi_{C_m}$ ) supermodes in the  $m$ th unit cell are in the form of  $|\Psi_m(0)\rangle \equiv (\psi_{D_m}, \psi_{C_m})^T = (e^{-(m-m_c)^2/(2\sigma^2)} e^{ikm} / \sqrt{4\pi\sigma^2}) |\psi_{i,+}(k)\rangle$ , where  $m_c = 0$  governs the center of the wave packet, and  $\sigma = 20$  controls the width of the wave packet.
- [75] The number of topological interface states formed at the spatial interface is the change in the winding number across the spatial interface,  $|w_i - w_f|$  [98–100].
- [76] Z. Huang and A. V. Balatsky, Dynamical quantum phase transitions: Role of topological nodes in wave function overlaps, *Phys. Rev. Lett.* **117**, 086802 (2016).
- [77] M. H. Mostafa, M. S. Mirmoosa, M. S. Sidorenko, V. S. Asadchy, and S. A. Tretyakov, Temporal interfaces in complex electromagnetic materials: an overview, *Opt. Mater. Exp.* **14**, 1103 (2024).
- [78] M. Aidelsburger, M. Lohse, C. Schweizer, M. Atala, J. T. Barreiro, S. Nascimbène, N. R. Cooper, I. Bloch, and N. Goldman, Measuring the Chern number of Hofstadter bands with ultracold bosonic atoms, *Nat. Phys.* **11**, 162 (2015).
- [79] M. Wimmer, H. M. Price, I. Carusotto, and U. Peschel, Experimental measurement of the Berry curvature from anomalous transport, *Nat. Phys.* **13**, 545 (2017).
- [80] M. Tarnowski, F. N. Ünal, N. Fläschner, B. S. Rem, A. Eckardt, K. Sengstock, and C. Weitenberg, Measuring topology from dynamics from obtaining the Chern number from a linking number, *Nat. Commun.* **10**, 1728 (2019).
- [81] D. Leykam and D. A. Smirnova, Probing bulk topological invariants using leaky photonic lattices, *Nat. Phys.* **17**, 632 (2021).
- [82] D. Leykam, E. Smolina, A. Maluckov, S. Flach, and D. A. Smirnova, Probing Band Topology Using Modulational Instability, *Phys. Rev. Lett.* **126**, 073901 (2021).
- [83] C. Chen, R.-Z. Liu, J. Wu, Z.-E. Su, X. Ding, J. Qin, L. Wang, W.-W. Zhang, Y. He, X.-L. Wang, C.-Y. Lu, L. Li, B. C. Sanders, X.-J. Liu, and J.-W. Pan, Berry Curvature and Bulk-Boundary Correspondence from Transport Measurement for Photonic Chern Bands, *Phys. Rev. Lett.* **131**, 133601 (2023).
- [84] D. Yu, B. Peng, X. Chen, X.-J. Liu, and L. Yuan, Topological holographic quench dynamics in a synthetic frequency dimension, *Light Sci. Appl.* **10**, 209 (2021).
- [85] T. Mizoguchi, Y. Kuno, and Y. Hatsugai, Detecting Bulk Topology of Quadrupolar Phase from Quench Dynamics, *Phys. Rev. Lett.* **126**, 016802 (2021).
- [86] X.-L. Zhang, F. Yu, Z.-G. Chen, Z.-N. Tian, Q.-D. Chen, H.-B. Sun, and G. Ma, Non-Abelian braiding on photonic chips, *Nat. Photon.* **16**, 390 (2022).
- [87] Y. Yang, B. Yang, G. Ma, J. Li, S. Zhang, and C. T. Chan, Non-Abelian physics in light and sound, *Science* **383**, 844 (2024).
- [88] D. Cheng, K. Wang, C. Roques-Carmes, E. Lustig, O. Y. Long, H. Wang, and S. Fan, Non-Abelian lattice gauge fields in photonic synthetic frequency dimensions, *Nature* **637**, 52 (2025).
- [89] D. Leykam and Y. D. Chong, Edge Solitons in Nonlinear-Photonic Topological Insulators, *Phys. Rev. Lett.* **117**, 143901 (2016).
- [90] D. Smirnova, D. Leykam, Y. Chong, and Y. Kivshar, Nonlinear topological photonics, *Appl. Phys. Rev.* **7**, 021306 (2020).
- [91] S. Mukherjee and M. C. Rechtsman, Observation of Unidirectional Solitonlike Edge States in Nonlinear Floquet Topological Insulators, *Phys. Rev. X* **11**, 041057 (2021).
- [92] G. Villa, J. del Pino, V. Dumont, G. Rastelli, M. Michalek, A. Eichler, and O. Zilberberg, Topological classification of driven-dissipative nonlinear systems, [arXiv:2406.16591](https://arxiv.org/abs/2406.16591).
- [93] T. Dai, Y. Ao, J. Mao, Y. Yang, Y. Zheng, C. Zhai, Y. Li, J. Yuan, B. Tang, Z. Li, J. Luo, W. Wang, X. Hu, Q. Gong, and J. Wang, Non-Hermitian topological phase transitions controlled by nonlinearity, *Nat. Phys.* **20**, 101 (2024).
- [94] A. Fritzsche, T. Biesenthal, L. J. Maczewsky, K. Becker, M. Ehrhardt, M. Heinrich, R. Thomale, Y. N. Joglekar, and A. Szameit, Parity-time-symmetric photonic topological insulator, *Nat. Mater.* **23**, 377 (2024).
- [95] Y. Sharabi, A. Dikopoltsev, E. Lustig, Y. Lumer, and M. Segev, Spatiotemporal photonic crystals, *Optica* **9**, 585 (2022).
- [96] Y. Peng, Topological Space-Time Crystal, *Phys. Rev. Lett.* **128**, 186802 (2022).
- [97] J. Feis, S. Weidemann, T. Sheppard, H. M. Price, and A. Szameit, Spacetime-topological events, [arXiv:2407.02176](https://arxiv.org/abs/2407.02176).
- [98] L. Lu, J. D. Joannopoulos, and M. Soljačić, Topological photonics, *Nat. Photonics* **8**, 821 (2014); Topological states in photonic systems, *Nat. Phys.* **12**, 626 (2016).

- [99] A. B. Khanikaev and G. Shvets, Two-dimensional topological photonics, *Nat. Photonics* **11**, 763 (2017).
- [100] Y. Wu, C. Li, X. Hu, Y. Ao, Y. Zhao, and Q. Gong, Applications of topological photonics in integrated photonic devices, *Adv. Opt. Mater.* **5**, 1700357 (2017).